PUBLICATIONS DE L'INSTITUT MATHÉMATIQUE
Nouvelle série, tome 111(125) (2022), 17–40 DOI: https://doi.org/10.2298/PIM2225017M

HAMILTONIAN SURFACES IN THE 4-CUBE, 4-BIT GRAY CODES AND VENN DIAGRAMS

Manuela Muzika Dizdarević and Rade T. Živaljević

Abstract. We study *Hamiltonian surfaces* in the d-dimensional cube I^d as intermediate objects useful for comparative analysis of *Venn diagrams* and *Gray cycles*. In particular we emphasize the importance of 0-Hamiltonian spheres and the "sphericity" of Gray codes in the context of *reducible* Venn diagrams. For illustration we show that precisely two, out of the nine known types of 4-bit Gray cycles, are not spherical. The unique, balanced Gray cycle is spherical, which in turn leads to a new construction of a reducible Venn diagram with 5 ellipses (originally constructed by P. Hamburger and R. E. Pippert).

1. Introduction

1.1. Gray codes and Hamiltonian surfaces. The idea of a *Hamiltonian circuit* in a graph can be naturally extended to higher-dimensional complexes.

Following [**15**] and [**5**], a subcomplex of a d-dimensional polyhedral complex P^d (for instance a subcomplex of a convex polytope) is called k-Hamiltonian if contains the full k-dimensional skeleton of P^d. In particular a k-Hamiltonian n-manifold in P^d is a k-Hamiltonian subcomplex of P^d which is at the same time an n-dimensional submanifold of P^d.

For example a 1-Hamiltonian 2-manifold (or 1-Hamiltonian surface for short) in the d-dimensional cube I^d is a polyhedral surface in I^d which contains all edges of the cube I^d. Similarly a 0-Hamiltonian surface in I^d contains all vertices of I^d and a 0-Hamiltonian 1-manifold in I^d is a Hamiltonian circuit (in the usual sense) in the vertex-edge graph of I^d.

Hamiltonian circuits in I^d are known also as *Gray cycles* (Gray codes), see [**14**, Section 7.2.1.1].

1.2. Venn diagrams. Following [**3**, **8**, **18**] a *Venn diagram* (or n-Venn diagram) in the plane (or on the sphere) is a collection of simple closed (Jordan) curves $\mathcal{F} = \{C_1, C_2, \dots, C_n\}$ such that each of the 2^n sets $X_1 \cap X_2 \cap \cdots \cap X_n$ is

2020 *Mathematics Subject Classification:* Primary 52B70; Secondary 05C45, 52B11.
Key words and phrases: Hamiltonian surfaces, Gray cycles, Venn diagrams.
Communicated by Stevan Pilipović.

non-empty and connected, where X_i is either the interior or the exterior of the curve C_i.

A *simple Venn diagram* is a Venn diagram with an additional property that no more than two curves intersect at a common point. A Venn diagram is *reducible* if one of the curves can be removed so that the remaining curves still form a Venn diagram. An n-Venn diagram is *extendible* if the addition of some curve results in an $(n+1)$-Venn diagram.

1.3. Winkler's conjecture and Gray cycles. *Winkler's conjecture* was originally proposed by Peter Winkler [**20**]. With a slight modification of Grünbaum [**9**] it reads as follows.

Winkler's conjecture. Every simple n-Venn diagram is extendible to a simple $(n+1)$-Venn diagram.

Gara Pruesse and Frank Ruskey announced a positive answer to Winkler's conjecture [**16**] in 2015. Previously it was demonstrated by Chilakamarri, Hamburger, and Pippert [**4**] in 1996 that the conjecture is true if the simplicity condition is removed.

A Venn diagram $\mathcal{F}$ can be regarded as a planar graph $V(\mathcal{F})$ (also referred to as the Venn diagram) in which the vertices are the points of intersection and edges are the segments of the curves between the vertices. In the Venn graph context, Winkler's question is equivalent to asking whether the planar dual $D(\mathcal{F})$ of a simple Venn diagram $V(\mathcal{F})$ is Hamiltonian.

If $\mathcal{F}$ is a simple d-Venn diagrams, then $D(\mathcal{F})$ is a subgraph of the vertex-edge graph $Q_d := \mathrm{Graph}(I^d)$ of the d-cube and, as a consequence, a Hamiltonian path in $D(\mathcal{F})$ is a Gray cycle.

Moreover, this Gray cycle is *spherical* in the sense that it can be covered by a 0-Hamiltonian sphere in I^d. Indeed $D(\mathcal{F})$, as a maximal bipartite planar graph, defines a quadrangulation of the sphere which is a subcomplex of I^d.

1.4. Which Gray cycles are spherical? Previous section illustrates the relevance of the sphericity of Gray cycles for the general question of extendability/reducibility of Venn diagrams.

The "binary reflected Gray code" [**14**, Section 7.2.1.1], one of the simplest Gray cycles, is clearly spherical. It is not a surprise that it emerges in many classical inductive constructions of Venn diagrams, see for examples [**18**], the section "Gray codes and Edwards' construction".

In summary, spherical Gray cycles may be useful in the construction and classification of new Venn diagrams. Motivated by these and other related questions we formulate the following general problem.

Problem. 1. Which Gray cycles in the d-cube I^d are spherical?

2. Given a not necessarily spherical Gray cycle Γ in I^d, determine the smallest genus of a 0-Hamiltonian surface in I^d which contains Γ.

The following theorem gives a complete answer in the case of the 4-dimensional cube I^4.

THEOREM 1.1. *There exist* 16 *different* 0*-Hamiltonian spheres in the* 4*-cube* I^4. *Up to a symmetry of* I^4 *they fall into two types referred to as* (P_1) *and* (P_3). *The first type arises as the quadrangulation of the sphere associated to the (unique)* 4*-Venn diagram on* S^2. *Following Gilbert* [**6**] *there are* 2688 *different Gray cycles in* I^4 *which are (Section* 4*) classified into 9 types, referred to as* G_1*–*G_9.

(a) *All Gray cycles* G_i*, with exception of* G_3 *and* G_4*, can be moved by an automorphism of the ambient* 4*-cube into a* 0*-Hamiltonian sphere of the type* (P_1).
(b) *Only the cycles* G_1, G_6, G_7, G_8 *and* G_9 *can be moved by an automorphism of the ambient* 4*-cube into a* 0*-Hamiltonian sphere of the type* (P_3).

It follows from Theorem 1.1 that the codes G_3 and G_4 are the only two 4-bit Gray cycles that are not spherical. Their genus is equal to 1 since they are both included in a *Karnaugh torus* (Section 3). From here we deduce (Section 6.2) that neither of the codes G_3 and G_4 is knotted in the boundary ∂I^4 of the 4-cube (for the remaining codes it is an immediate consequence of their sphericity).

1.5. Exceptional role of the Gray code G_9**.** The unique, balanced Gray cycle (Section 2), classified here as G_9, is spherical and corresponds (Section 6) to a unique Venn diagram, the "clown" diagram from [**12**]. In Section 7 we demonstrate how the properties of the balanced Gray cycle can be used for construction of a reducible Venn diagram with 5 ellipses (originally constructed in [**12**]). Finally in Section 8, we give a conceptual and a computer-independent proof of the existence and uniqueness of the balanced Gray cycle in dimension four.

2. The unique balanced 4-bit Gray code

The 4-bit Gray code exhibited as an array (matrix) (2.1) of column vectors is *balanced* in the sense that in each row the number of changes from 0 to 1, or vice versa, is the same (and equals to 4).

$$
\begin{array}{cccccccccccccccc}
0 & 1 & 1 & 0 & 0 & 0 & 1 & 1 & 1 & 1 & 1 & 1 & 0 & 0 & 0 & 0\\
0 & 0 & 1 & 1 & 1 & 1 & 1 & 1 & 0 & 0 & 0 & 1 & 1 & 0 & 0 & 0\\
0 & 0 & 0 & 0 & 1 & 1 & 1 & 1 & 1 & 1 & 0 & 0 & 0 & 0 & 1 & 1\\
0 & 0 & 0 & 0 & 0 & 1 & 1 & 0 & 0 & 1 & 1 & 1 & 1 & 1 & 1 & 0
\end{array}
\tag{2.1}
$$

It is an interesting and important fact that the balanced 4-bit Gray code is up to symmetry unique in dimension 4. This was first observed by Tootill [**19**], see also [**6**] and [**14**]. The proof of uniqueness relied on the computer generated list of all Gray codes of length 16. Indeed, as demonstrated in [**6**], there are 9 non-isomorphic 4-bit Gray codes, and precisely one of them is balanced.

There are results, such as [**23**, Theorem 5.1], whose proof critically depends on the uniqueness of the balanced, 4-bit Gray code. For this reason we give in Section 8 a conceptual proof of this fact, which does not depend on a computer search. We also demonstrate in Section 7 how the existence of this code leads directly to a construction of a *reducible Venn diagram*, consisting of five ellipses (see [**12, 13**] for the original construction).

Branko Grünbaum, a mathematician with great geometric insight, was the first to observe that a (non-reducible) Venn configuration of five ellipses exists [**8**, **9**], contrary to the belief of John Venn himself. He is also credited for the *Grünbaum–Hadwiger–Ramos* problem [**7**, **10**, **17**], which is in dimension 4 closely linked to the balanced, 4-bit Gray code [**17**, **24**].

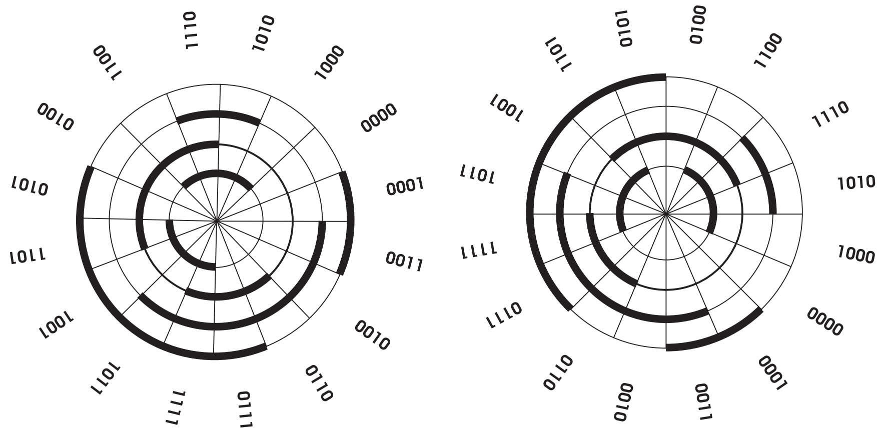

FIGURE 1. Two images of the balanced code. The image from [**14**] is on the left.

2.1. Inner symmetry of the balanced, 4-bit Gray code. An image of the balanced 4-digit Gray code (reproduced here in Figure 1 on the left) appears on page 293 in [**14**, Section 7.2.1.1]. By comparing this image with Figure 1 on the right, one observes that Knuth's image is rotated counterclockwise through the angle of $\frac{3\pi}{8}$.

The right image, taken from [**24**], reveals an additional symmetry of this code which was apparently not well known or emphasized before. For the reader's convenience these two representations are reproduced here in Figure 2 by the equivalent "polygonal representations".

Figure 2 on the right has the advantage that it clearly exhibits the vertical axes of symmetry of the balanced code which, in particular, explains why the same code is obtained if we read (2.1) (or (2.2)) backwards.

2.2. Remark on the notation. Another useful presentation of Gray codes puts more emphasis on edges, rather than on the vertices of the edge path. For example the balanced 4-bit Gray code exhibited in (2.1) can be also written as the sequence

$$1\quad 2\quad 1\quad 3\quad 4\quad 1\quad 4\quad 2\quad 4\quad 3\quad 2\quad 1\quad 2\quad 3\quad 4\quad 3 \tag{2.2}$$

recording the change of the corresponding coordinates. More geometrically, each edge of Q_4 (the vertex-edge graph of the 4-cube) is parallel to one of the coordinate axes (or the corresponding unit vectors e_1, e_2, e_3, e_4) in $\mathbb{R}^4$ and the sequence (2.2)

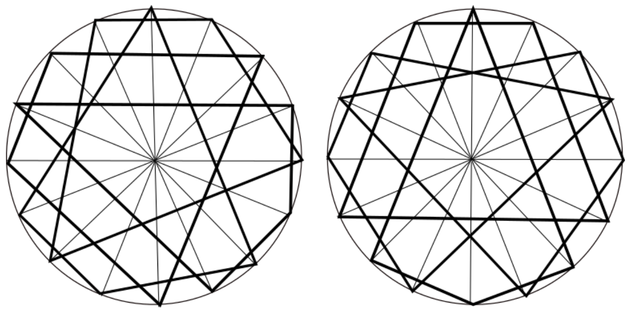

FIGURE 2. Hidden axes of symmetry of the balanced code

records the indices of these axes as they appear when we move along the Gray code. Note that the condition that the code is balanced becomes even more transparent as the property that each number (index) from $\{1, 2, 3, 4\}$ appears precisely four times.

REMARK 2.1. Strictly speaking a d-Gray cycle is a subgraph $\Gamma \subset Q_d$ isomorphic to a cycle of length 2^d. The associated cyclic word C-word(Γ) in the alphabet $[d] = \{1, \dots, d\}$ records the intersections $\Gamma \cap \{x = (x_i) \in I^d \mid x_i = 1/2\}$ of the Gray cycle with the corresponding halving hyperplanes of the d-cube.

The code words such as (2.2) arise when we choose an initial vertex on Γ and an orientation (preferred direction) of Γ.

More precisely the cyclic word C-word(Γ) associated to Γ is a cycle graph of length 2^d with the edges labeled by $1, 2 \dots, d$. Two cyclic words are considered to be equivalent (equal) if one of them is obtained from the other by an automorphism of the corresponding cycle graphs.

A basic observation is that two Gray cycles Γ_1 and Γ_2 are isomorphic if and only if the corresponding cyclic words C-word(Γ_1) and C-word(Γ_2) are equivalent (equal).

3. 1-Hamiltonian surfaces and the Karnaugh map

A 1-Hamiltonian surface, introduced in Section 1.1, is a 2-dimensional analogue of the Hamiltonian circuit. Less formally a 1-Hamiltonian surface in the d-dimensional cube I^d is a union M of 2-dimensional faces of the d-cube such that:

(1) M is an orientable 2-dimensional surface,
(2) M contains each edge of the cube I^d.

The second condition implies that Q_d, the vertex-edge graph of the d-cube, is embedded in the surface M. Moreover each face (a connected component of the graph complement in the surface) is a quadrangle. (Such decompositions of surfaces are called quadrangulations.)

A nice and useful consequence of (1) and (2) is that Hamiltonian circuits in I^d can be visualized (and studied) as Hamiltonian cycles in a quadrangulated surface. A classical example, originally used for the design of switching circuits, is the

Karnaugh map [**14**], defined as a quadrangulation of the 2-dimensional torus $T^2 = S^1 \times S^1$.

More explicitly if $S^1 = \partial I^2$ is the boundary of the square, then the Karnaugh torus is the quadrangulated surface $K = \partial I^2 \times \partial I^2$, interpreted as a 1-Hamiltonian surface in the 4-cube, via the embedding $\partial I^2 \times \partial I^2 \hookrightarrow I^2 \times I^2 = I^4$.

Karnaugh torus is depicted in Figure 3 (on the left) together with the balanced Gray code described by the associated code word from equation (2.2).

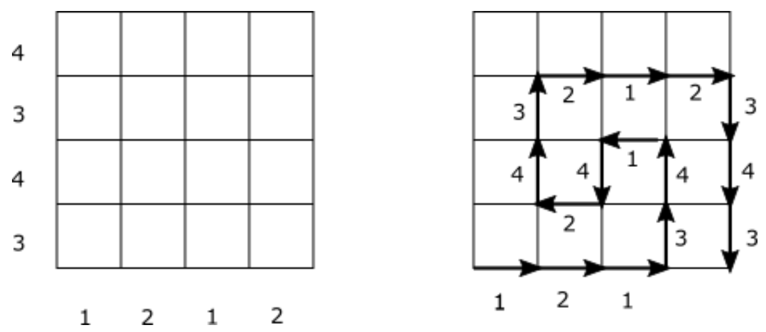

FIGURE 3. Karnaugh map and the balanced, 4-bit Gray code

It is natural to ask for a 1-Hamiltonian surface $M = M_g$ in I^d of the smallest possible genus g; in particular to decide if there exists a 1-Hamiltonian sphere in I^4. These questions are related to the problem of finding the genus of the cube graph Q_d, that is the minimum g such that Q_d admits an embedding in M_g. The well known answer is given by the following classical result of Ringel and (independently) of Beineke and Harary.

THEOREM 3.1. [**11**, Theorem 11.20] *The genus of the d-cube graph is*

$$g(Q_d) = 1 + (d-4)2^{d-3}\,.$$

From here we immediately deduce that $g(Q_4) = 1$ which implies that a 1-Hamiltonian sphere does not exist already in the case $d = 4$. Moreover, there is a relation ([**11**, Corollary 11.1 (b)])

$$f_1 = 2f_0 - 4 \tag{3.1}$$

which holds for all quadrangulations of the 2-sphere with f_0 vertices and f_1 edges. It immediately follows that each quadrangulated 2-sphere with $f_0 = 16$ vertices must have $f_1 = 28$ edges, see Figure 8 for an examples. In other words each 2-sphere $\Gamma \subset I^4$ which is 0-Hamiltonian, in the sense that it contains all vertices of I^4, is 4 edges short from being a Hamiltonian (1-Hamiltonian) surface in I^4.

This observation serves as a motivation for asking if for each Hamiltonian circuit H there exists a 0-Hamiltonian 2-sphere Γ in I^4 such that $H \subset \Gamma$.

Theorem 1.1 provides a negative answer to this question. The proof is, after some preparation, given in Section 6.

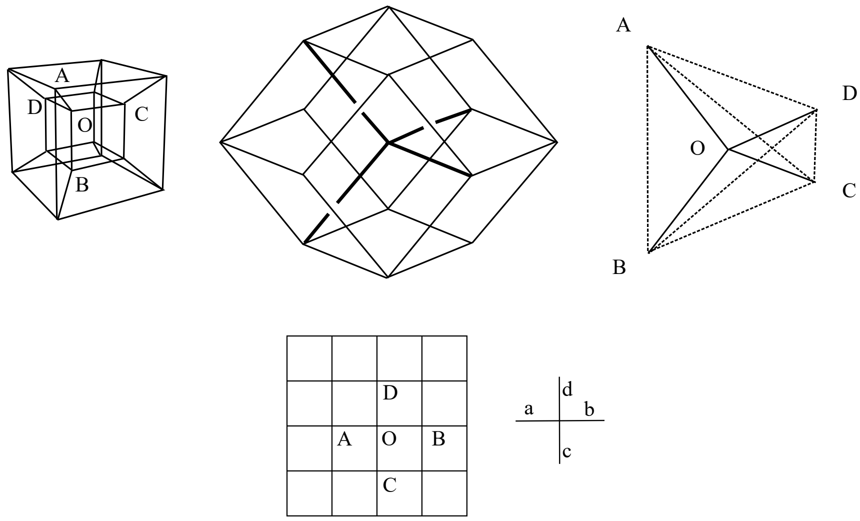

FIGURE 4. The uniqueness of the Karnaugh torus.

3.1. The uniqueness of the Karnaugh torus.

PROPOSITION 3.1. *The Karnaugh torus is essentially the only* 1*-Hamiltonian quadrangulated surface embedded in the* 4*-cube* I^4*. More precisely, if* M *is a* 1*-Hamiltonian quadrangulated surface embedded in the* 4*-cube* I^4*, then there is an automorphism of the cube* I^4 *which maps* M *to the standard Karnaugh torus depicted in Figure 3.*

PROOF. Each vertex O of the 4-cube (Tesseract) is a common vertex of six squares incident to O (Figure 4). Rhombic dodecahedron, defined as the Minkowski sum of 4 segments (OA, OB, OC and OD), is depicted in the middle of this figure. It provides an accurate model of the neighborhood N of O in I^4, as far as the 2-dimensional skeleton of the 4-cube is concerned.

From this model we easily read off the local structure of all possible surfaces, subcomplexes of I^4, which have O as a vertex. If O is a 4-valent vertex in M then there are 3 possibilities for the intersection $M \cap N$, while if O is 3-valent in M there are 4 possible local models for M.

These local models correspond to different cycles in the 1-skeleton of the tetrahedron $ABCD$. For example the cycle AC-CB-BD-DA corresponds to the neighborhood of O of the Karnaugh torus K depicted at the bottom of Figure 4.

Suppose that M is a 1-Hamiltonian surface in I^4 and let $O \in M$ be a chosen vertex. Using the symmetries of the 4-cube we may assume that the neighborhood of O in M is described by the cycle AC-CB-BD-DA, meaning that in the neighborhood of O the surface M coincides with the Karnaugh torus K.

Inductively we show that M and K coincide over a larger and larger fragment of K. Here we use the fact that all vertices of M are 4-valent (see Theorem 3.1). The induction step is based on the observation that for each two adjacent squares incident to a (variable) vertex O, such as the squares which share the edge OA of K (Figure 4), there is only one (out of 3) local models containing these squares. (In our example it is the model corresponding to the cycle AC-CB-BD-DA.)

Summarizing, we observe that if M contains the squares in K incident to the edge OA it also contains the two squares in K sharing the edge OB, etc. This procedure continues until we obtain that $M = K$. □

3.2. Surgery over the Karnaugh torus. Let M_1 be the union of 7 quadrangles (squares) in the Karnaugh torus K, depicted as the shaded region in Figure 5.

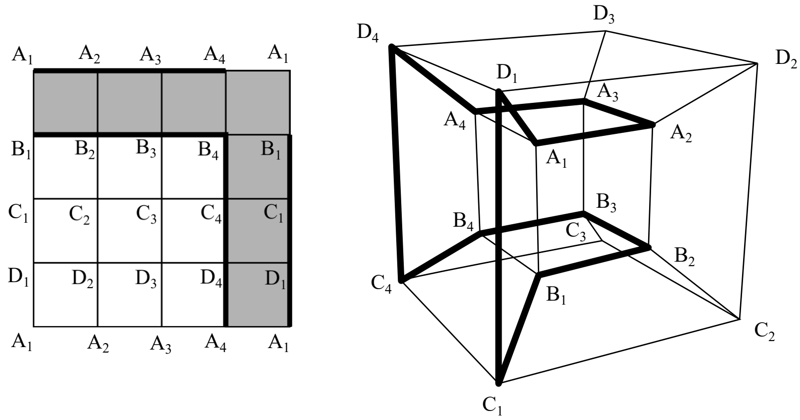

FIGURE 5. A surgery on the Karnaugh torus.

By inspection we observe that M_1 is a 2-dimensional surface with the boundary $\Gamma = A_1A_2A_3 \dots C_1D_1A_1$ consisting of 12 line segments, as shown in Figure 5 on the right. The union of the remaining 9 squares (the non-shaded 3×3-chessboard in Figure 5) is a topological disk U, also bounded by Γ. The union V of 5 squares

$$A_1A_2A_3A_4, A_1B_1C_1D_1, A_4B_4C_4D_4, B_1B_2B_3B_4, A_1B_1B_4A_4$$

is also a topological disc with boundary Γ. The discs U and V have disjoint interiors, hence the union $W := U \cup V$ is a sphere quadrangulated into 14 squares. This quadrangulation has 16 vertices which implies that W is a 0-Hamiltonian sphere in the 4-cube I^4. As predicted by the relation (3.1) precisely 4 edges from the Karnaugh torus are not in W, namely the edges

$$A_2B_2, A_3B_3, C_1C_4, D_1D_4\,. \tag{3.2}$$

It is convenient to represent the quadrangulated sphere W, as the planar map (graph) shown in Figure 6. Note that a similar (isomorphic) sphere can be constructed by a surgery over K if we choose (for the shaded region) a different row and a column in the 4×4-chessboard, associated to the Karnaugh torus (Figure 5).

As and immediate consequence we obtain the following result.

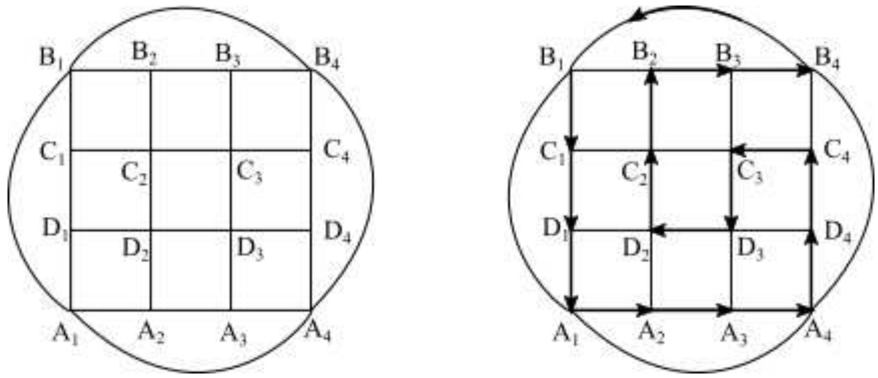

FIGURE 6. A balanced Gray code inside the sphere W.

PROPOSITION 3.2. *A balanced Gray code can be constructed within the* 0-*Hamiltonian sphere* W*, obtained by a surgery over the Karnaugh torus. In other words the balanced* 4-*bit Gray code is spherical (Section 1.3).*

PROOF. The balanced Gray code G exhibited in Figure 3 (on the right) has this property. Indeed, none of the edges listed in (3.2) is traversed by this code, hence $\Gamma \subset W$. An explicit realization is given in Figure 6 on the right. $\square$

4. Nine Hamiltonian cycles in I^4

Here for the future reference we reproduce the list [**6**, Table I] of all essentially different, 4-bit Gray cycles.

	G_1	1 2 1 3 1 2 1 (4) 1 2 1 3 1 2 1 (4)	$(8,4,2,2)$
	G_2	1 2 1 3 1 2 1 (4) 2 1 2 3 2 1 2 (4)	$(6,6,2,2)$
	G_3	1 2 1 3 2 1 2 (4) 1 2 1 3 2 1 2 (4)	$(6,6,2,2)$
	G_4	1 2 1 3 2 1 2 (4) 2 3 2 1 3 2 3 (4)	$(4,6,4,2)$
(4.1)	G_5	1 2 1 3 2 1 2 (4) 3 2 3 1 2 3 2 (4)	$(4,6,4,2)$
	G_6	1 2 3 2 1 2 3 (4) 3 2 1 2 3 2 1 (4)	$(4,6,4,2)$
	G_7	1 2 3 2 1 2 3 (4) 1 2 3 2 1 2 3 (4)	$(4,6,4,2)$
	G_8	1 2 3 2 1 2 3 (4) 1 3 1 2 1 3 1 (4)	$(6,4,4,2)$
	G_9	1 2 1 3 4 1 4 2 4 3 2 1 2 3 4 3	$(4,4,4,4)$

The type of the code G_i is the vector $Type(G_i) = (p_1, p_2, p_3, p_4)$, or more accurately a partition $16 = p_1 + p_2 + p_3 + p_4$ (the order of summands is not important), where p_j is the number of occurrences of the letter $j \in \{1, 2, 3, 4\}$ in the code. We use parentheses (such as (4) in the list above) for better visibility and to indicate a letter which occurs only two times.

4.1. Recognition of 4-bit Gray codes. It is known [**14**, Ch. 7.2.1.1] that there are 2688 different Gray cycles in Q_4. We need an efficient algorithm (recognition principle) which allows us to classify them into 9 equivalence classes of isomorphic codes. In other words, given a Gray code Γ, we need a test (as simple as possible) which allows us to determine the unique G_i from the list (4.1) isomorphic to Γ.

Step I. Classified by type, the Gray codes listed in (4.1) fall into four classes

$$A = \{G_1\} \quad B = \{G_2, G_3\} \quad C = \{G_4, G_5, G_6, G_7, G_8\} \quad D = \{G_9\}\,. \tag{4.2}$$

It follows that the type $Type(\Gamma)$ alone is sufficient to detect codes G_1 and G_9.

Step II. Number 2 appears as a summand in all the types except in $Type(G_9)$. As a consequence each of the codes G_2-G_8 has a (cyclic) representation of the form $w_1(4)w_2(4)$ (or $w_1(3)w_2(3)$), where w_1 and w_2 are words describing a Hamiltonian path in a 3-cube.

The only vectors (p, q, r) that appear as types of Hamiltonian paths in a 3-cube are

$$U = (4, 2, 1) \quad V = (3, 2, 2) \quad W = (3, 3, 1)\,. \tag{4.3}$$

The first two are types of "broken cycles" (Hamiltonian paths in a 3-cube connecting two neighboring vertices) while W is the type of the "backbone" Hamiltonian path which connects two diametrically opposite vertices.

The vectors (4.3) are referred to as ***subtypes*** of a Gray cycle and Subtype(Γ) is the collection of all subtypes of Γ. By inspection we observe that

$$\mathrm{Subtype}(G_2) = \{U, W\} \quad \mathrm{Subtype}(G_3) = \{W\}$$

which means that the appearance of the subtype U is characteristic for G_2. By a similar analysis the class C splits as follows,

$$\mathrm{Subtype}(G_4) = \mathrm{Subtype}(G_5) = \{W\}$$
$$\mathrm{Subtype}(G_6) = \mathrm{Subtype}(G_7) = \{V\}$$
$$\mathrm{Subtype}(G_8) = \{U, V\}$$

Step III. It remains to separate G_4 from G_5 and G_6 from G_7. This is done by comparing the words w_1 and w_2 in the cyclic representations $w_1(4)w_2(4)$ of these codes.

In the case of G_7 these words are identical, $w_1 = w_2$. In the case of G_6 these words are different. More precisely they are conjugate $w_1 \neq w_2 = \overline{w}_1$, in the sense that one is obtained from the other by reading the first word in the opposite order.

In the case of G_4 we have $w_1 = 1213212$ and $w_2 = 2321323$ (more generally $w_1 = xyxzyxy$ and $w_2 = yzyxzyz$ for a code isomorphic to G_4), which means that the Hamming distance of these two strings is 7 (they are different in all bit positions).

In the case of G_5 we have $w_1 = 1213212$ and $w_2 = 3231232$ (or in general $w_1 = xyxzyxy$ and $w_2 = zyzxyzy$), which means that the Hamming distance $Hamm(w_1, w_2)$ of these two strings is 4 (they are equal in three bit positions).

5. A classification of 0-Hamiltonian spheres in I^4

In this section we classify up to symmetry of the 4-cube all 0-Hamiltonian spheres in I^4. It turns out that they fall into two different isomorphism types, (P_1) and (P_3), as shown in Figure 7 (see also Figure 8 for the corresponding spherical realizations).

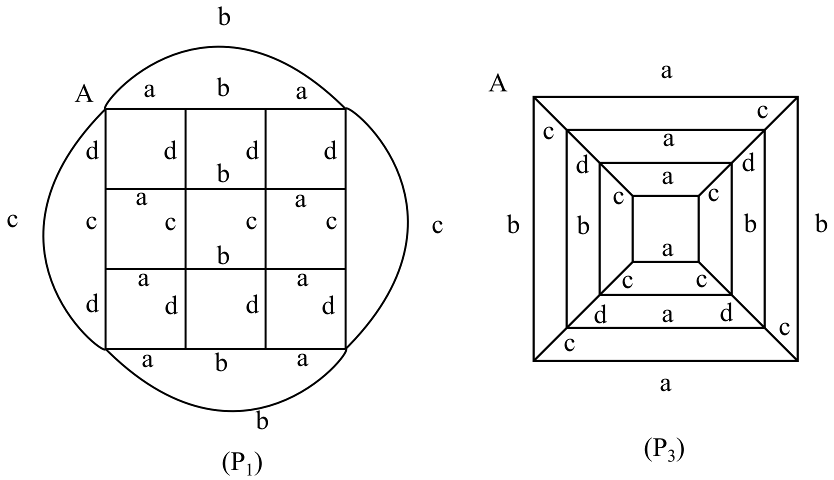

FIGURE 7. Two 0-Hamiltonian spheres in the 4-cube.

PROPOSITION 5.1. *There are only two essentially different* 0*-Hamiltonian spheres in* I^4.

PROOF. Let M be a 0-Hamiltonian sphere in I^4. It follows from Section 3 that M is a quadrangulation of the 2-sphere with 16 vertices, 28 edges and 14 quadrangular faces. Suppose that v_i is the number of vertices of degree i. Since all vertices are either of degree 3 or degree 4, we have the relations

$$v_3 + v_4 = 16, \qquad 3v_3 + 4v_4 = 56\,.$$

As an immediate consequence we obtain that the numbers of 3-valent and 4-valent vertices is $v_3 = v_4 = 8$.

Altogether there are 32 edges in I^4 divided into 4 parallel classes, each class with 8 edges. If e_1 and e_2 are two edges in M, we say that they are P-equivalent if they are in the same parallel class and there is a sequence

$$e_1 = z_1, z_2, \dots, z_{k-1}, z_k = e_2$$

of edges in M such that z_i and z_{i+1} are opposite edges in a quadrangle q_i of M, for each $i \leqslant k-1$

The equivalence classes of P-equivalent edges of M are called *belts*, since the quadrangles $\{q_i\}_{i=1}^k$ form a “belt” on the surface M. The number k is referred to as the length of the belt.

Since the cycles in I^4 are of even length, the length of a belt is an even number $4 \leqslant l \leqslant 8$. If b_i is the number of different belts of length i then

$$4b_4 + 6b_6 + 8b_8 = 28. \tag{5.1}$$

If $b_8 \neq 0$, i.e., if there exists a belt of length 8, then M is isomorphic to either the first or the third quadrangulation depicted in Figure 8. Indeed, there are altogether

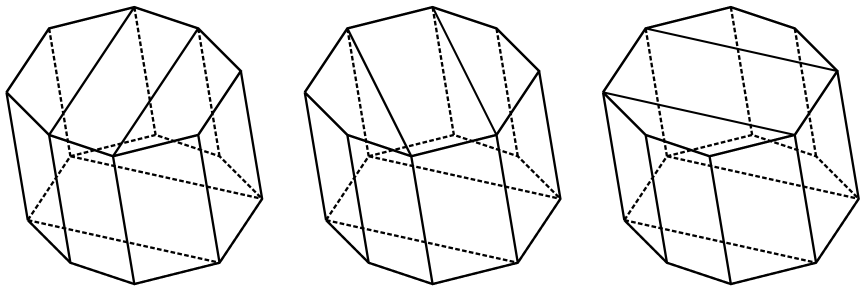

(P1) (P2) (P3)

FIGURE 8. Three potential 0-Hamiltonian spheres in I^4.

16 vertices in M and all of them are on the belt. The boundary of the belt consists of two connected components, each spanning an octagon. These two octagons are quadrangulated without new vertices, which immediately leads to the conclusion that M is one of the three quadrangulated surfaces depicted in Figure 8. The surface P_2 cannot be embedded in the 4-cube since it has a self-intersecting belt. The surfaces P_1 and P_3 are not isomorphic since $b_4(P_1) = 0 \neq 3 = b_4(P_2)$ and $b_6(P_1) = 2 \neq b_6(P_2) = 0$ ($b_8(P_1) = b_8(P_2) = 2$).

We continue by analysing the case $b_6 \neq 0$. Let B a belt of length 6 and B_1 and B_2 its boundary 6-gons. Each cycle in I^4 of length 6 is contained in a 3-dimensional face of I^4. Indeed, each parallel class is in each cycle is represented by an even number of edges. It follows that the word in the alphabet $\{a, b, c, d\} = \{1, 2, 3, 4\}$ associated to a 6-cycle is either $w_1 = abcacb$ or $w_2 = abcabc$. The word $w_1 = abcacb$ is realized in the quadrangulation depicted in Figure 9 and this is, up to symmetry of I^4, the only realization. Moreover, this quadrangulation, the quadrangulation (P_1) and the quadrangulation depicted in Figure 6 (on the left) are all isomorphic. This can be observed by tracking and comparing the belts of length 8 in all three quadrangulations.

The word $w_2 = abcabc$ cannot arise as the word associated to a boundary cycle B_1 (or B_2) of a 6-belt B in a 0-Hamiltonian surface M. Formally, the associated quadrangulation would appear (as a graph) similar to Figure 9, but with different labeling (described by the word w_2) of the two hexagonal bases. This labeling forces the edge in the middle of each of the hexagons to be labeled by d, which is contradiction.

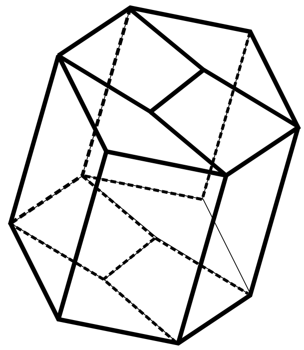

FIGURE 9. A 0-Hamiltonian sphere with $b_6 \neq 0$.

We conclude the analysis by showing that the remaining case $b_6 = b_8 = 0$ and $b_4 = 7$ is not possible. Indeed, in this case there would exist two distinct belts U and V of length 4 which share two quadrangles. However, this can happen only if the ambient sphere is the boundary of a 3-cube. □

6. Hamiltonian cycles inside 0-Hamiltonian spheres

PROPOSITION 6.1. *All Gray cycles listed in Section 4, with exception of G_3 and G_4, can be moved by an automorphism of the ambient 4-cube into a 0-Hamiltonian sphere of the type (P_1).*

PROOF. A generic 0-Hamiltonian sphere of the type (P_1) in the 4-cube is exhibited in Figure 7, where A is a vertex in I^4 and $\{a, b, c, d\} = \{1, 2, 3, 4\}$.

The vertex-edge graph of (P_1) has been already studied in **[12]** as the dual graph of the unique 4-Venn diagram on the sphere. In particular Hamburger and Pippert listed 11 different types of Hamiltonian cycles in this graph (see Theorem 4.1 and Figures 3 and 4 in [**12**]).

We use these 11 Hamiltonian cycles (listed as $H_1, \ldots, H_{11}$), together with the algorithm described in Section 4.1, to describe all Gray cycles which can be covered by a sphere of type (P_1). Initially we read off the code word (in the alphabet $\{a, b, c, d\}$) associated to each of the cycles H_i by tracking this cycle in Figure 7 in clockwise direction, starting at the vertex A. After that we use the recognition algorithm to detect the corresponding G_j. □

6.1. The case of P_3-spheres.

PROPOSITION 6.2. *Among all Gray cycles listed in Section 4, only the cycles G_1, G_6, G_7, G_8 and G_9 can be moved by an automorphism of the ambient 4-cube into a 0-Hamiltonian sphere of the type (P_3).*

PROOF. The proof in principle could be given along the lines of the proof of Proposition 6.1. To carry on that plan we would need a list of essentially different Hamiltonian cycles in the P_3-graph (Figure 7).

(H_1) Codeword: $abacdcabcbdbadcd$
Type $(4,4,4,4)$
Conclusion: $H_1 \mapsto G_9$

(H_2) Codeword: $abadacadabadacad$
Type $(8,2,2,4)$
Conclusion: $H_2 \mapsto G_1$

(H_3) Codeword: $abadab(c)badabad(c)d$
Type $(6,4,2,4)$
Subtype=$\{V\}$, $w_2 = \overline{w}_1$
Conclusion: $H_3 \mapsto G_6$

(H_4) Codeword: $babdba(c)abdbabd(c)d$
Type $(4,6,2,4)$
Subtype=$\{V\}$, $w_2 = \overline{w}_1$
Conclusion: $H_4 \mapsto G_6$

(H_5) Codeword: $bd(c)dadbdad(c)abdba$
Type $(4,4,2,6)$
Subtype=$\{U,W\}$, $w_2 = \overline{w}_1$
Conclusion: $H_5 \mapsto G_8$

(H_6) Codeword: $ad(b)dad[c]ada(b)ada[c]d$
Type $(6,2,2,6)$
Subtype=$\{U,W\}$
Conclusion: $H_6 \mapsto G_2$

(H_7) Codeword: $bdc(a)cdbdcdb(a)bdcd$
Type $(2,4,4,6)$
Subtype=$\{V\}$, $w_2 = \overline{w}_1$
Conclusion: $H_7 \mapsto G_6$

(H_8) Codeword: $bdcdadcbdbcdadcd$
Type $(2,2,4,8)$
Conclusion: $H_8 \mapsto G_1$

(H_9) Codeword: $dcacd(b)acdcacd(b)ac$
Type $(4,2,6,4)$
Subtype=$\{V\}$, $w_1 = w_2$
Conclusion: $H_9 \mapsto G_7$

(H_{10}) Codeword: $bdadbd(c)badabad(c)d$
Type $(4,4,2,6)$
Subtype=$\{U,V\}$
Conclusion: $H_{10} \mapsto G_8$

(H_{11}) Codeword: $aba(d)cacbaca(d)babc$
Type $(6,4,4,2)$
Subtype=$\{W\}$, $Hamm(w_1,w_2) = 4$
Conclusion: $H_{11} \mapsto G_5$

Instead, here we use the idea implicitly used in the proof of Proposition 3.2.

LEMMA 6.1. *There are 8 different spheres of the type P_3 in the 4-cube I^4. They are in a one-to-one correspondence with rows and columns of the Karnaugh torus (Figure 3). More precisely, for each sphere in I^4 of the type P_3 the corresponding "missing edges" from the Karnaugh torus are all located either in the sam raw or in the same column.*

The proof of the proposition is completed by inspection of Figures 3 and 10. For example the balanced Gray cycle depicted in Figure 3 does not use the edges from the first row. Similarly the image of the Gray cycle of the type G_6, shown in Figure 10, does not contain any of the edges from the third column.

On the contrary each of the codes G_2, G_3, G_4, G_5 contains an edge from each of the rows (columns). Therefore none of these codes can be covered by a sphere of the type P_3. □

6.2. Are there non-trivial knots among Gray codes? The boundary $\partial(I^4)$ of the 4-dimensional cube is a 3-sphere so it is a legitimate question whether some of the 4-bit Gray codes is a non-trivial knot. Recall that the question of the existence of non-trivial knots in boundaries of 4-polytopes has a quite interesting history [**22**].

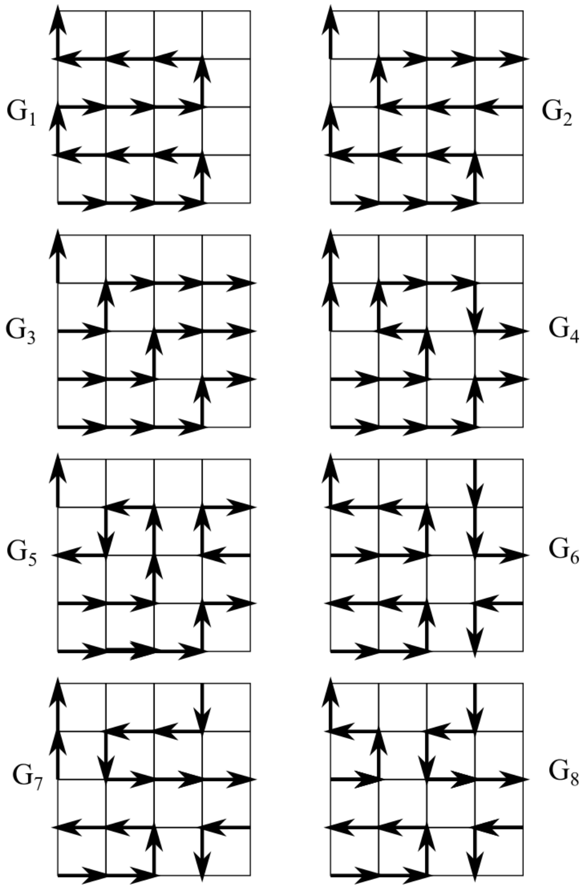

FIGURE 10. Hamilton paths G_1 to G_8 in the Karnaugh torus.

PROPOSITION 6.3. *Neither of the 9 Gray codes listed in [6] is knotted.*

PROOF. As an immediate consequence of Proposition 6.1, we observe that all Gray cycles G_i for $i \notin \{3,4\}$ are trivial knots. Indeed, each of them is embedded in a 2-sphere of the type (P_1) and by the Jordan curve theorem it bounds a disc.

For G_3 and G_4 we need a different argument. By inspection of Figure 10, we observe that G_3 is a torus knot of the type $(3,1)$, meaning that it winds three times horizontally and one time vertically in the Karnaugh torus. Similarly G_4 is a $(2,1)$-torus knot. It is a well known fact that a (p,q)-torus knot, where p and q are coprime integers, is a trivial knot if and only if either $p = \pm 1$ or $q = \pm 1$. $\square$

6.3. The "clown" configuration. As already observed in the proof of Proposition 6.1, among the 11 distinct, reducible spherical Venn diagrams with 5 curves (listed in [**12**, Theorem 4.1]), there is precisely one of them, the diagram H_1, which realizes the balanced Gray cycle.

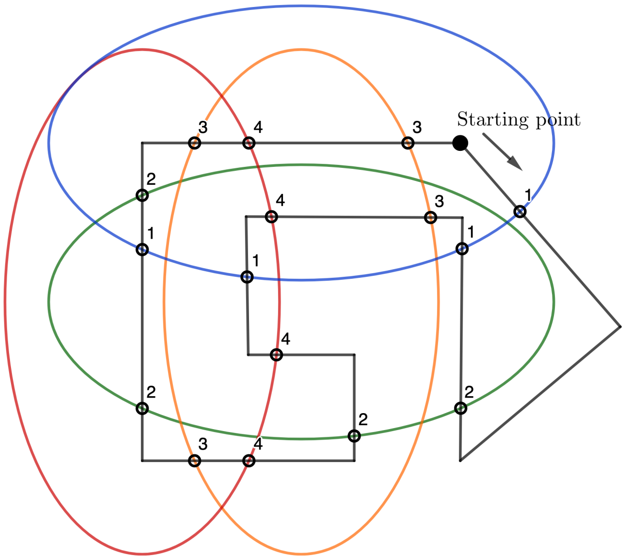

FIGURE 11. The "clown" configuration.

This Venn diagram, the "clown", as it is called in [**12**], is reproduced here in Figure 11.

7. Venn thought it couldn't be done

Here we use the unique, balanced 4-bit Gray code to describe a conceptual approach to the construction of a (reducible) planar Venn diagram consisting of five ellipses. Recall that J. Venn himself thought that a diagram with five ellipses does not exist and it came as a surprise when B. Grünbaum constructed [**8**] a configuration of ellipses with this property.

It is interesting that Grünbaum also made an oversight [**9**] (see also [**13**]) by claiming that "nor simple (in the sense that no 3 ellipses intersect) Venn diagram with five ellipses can be obtained by adding a fifth ellipse to a Venn diagram of four ellipses" (such diagrams are called reducible).

We refer the reader to [**12**, **13**] for a very interesting history of this problem and to [**3**, **12**, **13**] for far reaching results and numerous examples of Venn diagrams with curves of different shapes.

Our basic idea, for a construction of a reducible Venn diagram with five ellipses, is to use Figure 14. More explicitly, we will circumscribe ellipses around each of the four polygons inscribed in the circle to obtain four ellipses which, together with the circle, are expected to form a 5-Venn diagram. This is, however, not always the case and the ellipses must be chosen with some care.

Recall that a *pencil of conics* is a one-parameter family of conics which all pass through four given points. Therefore our goal is to choose carefully an ellipse in each of the four pencils, corresponding to four polygons inscribed in the circle.

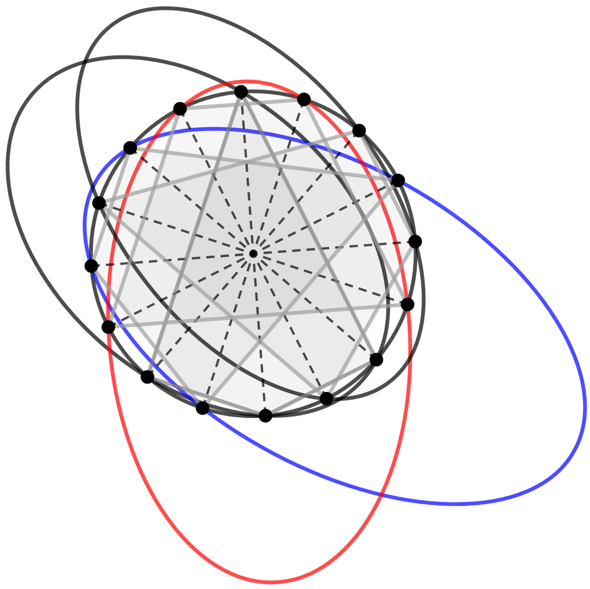

FIGURE 12. Five ellipses which form a reducible Venn diagram.

PROPOSITION 7.1. *Let $\{E_i\}_{i=1}^4$ a collection of ellipses chosen from the pencils of conics associated to the four polygons inscribed in the circle C depicted in Figure 14. Then the collection $\mathcal{F} = \{C, E_1, E_2, E_3, E_4\}$ is a Venn diagram if the ellipses $\mathcal{E} = \{E_1, E_2, E_3, E_4\}$ form a simple 4-Venn diagram.*

PROOF. Since $\mathcal{E} = \{E_1, E_2, E_3, E_4\}$ is a 4-Venn diagram, it divides the plane (sphere) into 16 connected components. Each of these components is bisected into two connected regions by one of the 16 arcs on the circle C. Therefore $\mathcal{F} = \{C, E_1, E_2, E_3, E_4\}$ is a 5-Venn diagram. □

A simple argument based on the Euler formula guarantees that a collection of ellipses $\mathcal{E} = \{E_1, E_2, E_3, E_4\}$ is a 4-Venn diagram if and only if

(1) Two ellipses, say E_1 and E_2, have four points in common;
(2) For any other pair $\{i, j\} \neq \{1, 2\}$ of indices, the ellipses E_i and E_j intersect in precisely two points.

Guided by these properties, with little experimentation, one obtains the diagram exhibited in Figure 12. The reader is referred to [**12**] for a fairly complete analysis of this problem, leading in particular to examples of reducible Venn diagrams formed by five congruent ellipses.

8. The uniqueness of the balanced 4-bit Gray code

The uniqueness of the balanced 4-bit Gray code is established in [**6**] by a computer search. Considering how important this fact is for applications such as [**23**], here we give a proof based on a simple case analysis.

If Γ is an arbitrary balanced 4-bit Gray code, such as (2.2), it can be visualized in two parallel 3-cubes $I^3_{(0)}$ and $I^3_{(1)}$, representing the front face and the back face of the 4-cube I^4. Note that in this representation the step in the direction of the coordinate vector e_4 corresponds to the "jump" (parallel translation) from $I^3_{(0)}$ to $I^3_{(1)}$ or vice versa.

If we remove letter $d = 4$ from (2.2), we obtain four words $w_i = w_i(\Gamma)\,(i = 1, 2, 3, 4)$ in the alphabet $\{1, 2, 3\}$ which will be referred to as *characteristic words* associated to Γ. A characteristic word is *principal* if it has the largest length. For example in (2.2), a (non-unique) principal word is $w = 32123$ and after a cyclic permutation (corresponding to a different choice of the initial vertex) we obtain the following representation of the code (2.2):

$$\Gamma = 32123(4)31213(4)1(4)2(4) = w_1(d)w_2(d)w_3(d)w_4(d)\,. \tag{8.1}$$

We sometimes write $w = \overset{--\to}{ST}$ if we want to emphasize that S is the *source* (initial vertex) and T the *sink* (terminal vertex) of the edge-path corresponding to ω.

In what follows a, b, c, d are tacitly assumed to be different elements in $\{1, 2, 3, 4\}$ where (most of the time) $d = 4$. The total length of all four characteristic words is 12 (so the average length is 3). It follows that the length of a principal word in a balanced, 4-bit Gray code, is five, four or three. We begin our analysis with the principal words of the length five.

8.1. Principal word of the type ***abcba*****.** Assume that $w_1 = abcba$ (where $\{a, b, c\} = \{1, 2, 3\}$) is a principal word associated to a balanced 4-bit Gray code Γ and that the remaining characteristic words are w_2, w_3, w_4. By symmetry we can assume that $a = 1$, $b = 3$, $c = 2$ which means that the initial (known) part of Γ is as shown in Figure 13 on the left.

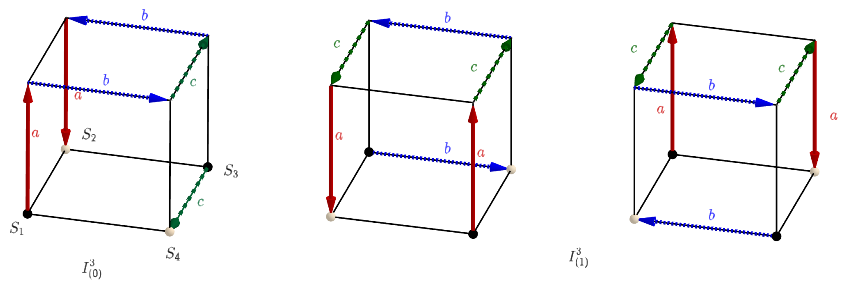

FIGURE 13. Principal word of the type *abcba*.

We immediately observe from Figure 13 that the characteristic word (path) w_3 must connect vertices S_3 and S_4, i.e., $w_3 = c$. It may not be immediately clear what is the source (sink) of w_3. However, a moment's reflections reveals that S_3 must be the source. Indeed, in the opposite case it would not be possible to construct characteristic paths w_2 and w_4 (in the back face $I^3_{(1)}$) which are disjoint.

There are precisely two ways to complete $w_1 = abcba$ (and w_3 with end-points S_3, S_4) to a Gray code on I^4. The corresponding characteristic words w_2 and w_4 are exhibited in Figure 13 on the right. Both these codes are balanced so we have established the existence of a balanced, 4-bit Gray code.

We observe that 32123 is a principal word of the type *abcba* in the code (2.2). It immediately follows that the two codes exhibited in Figure 13 are (up to symmetry) isomorphic either to (2.2) or to the same code read backwards.

Remark 8.1. Perhaps the easiest way to show that both balanced codes constructed in Section 8.1 are isomorphic to the code (2.2) (and its reversal) is to visualise (interpret) them in Figure 14 (labeled version of Figure 2 on the right). The reflection with respect to the major diagonal of the deltoid keeps both the deltoid and the trapeze invariant, while interchanging the remaining two (congruent) quadrangles. From here we immediately deduce that this code is isomorphic to the same code read backwards.

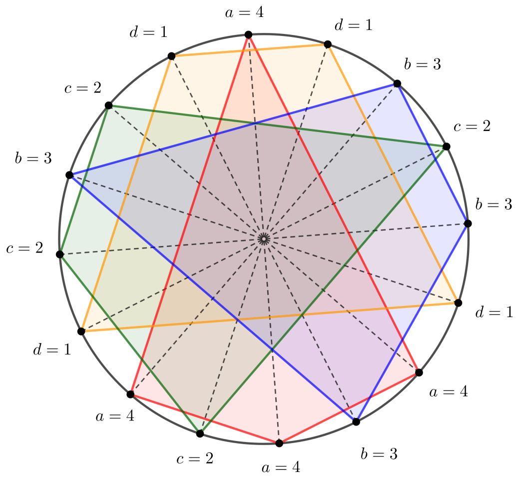

Figure 14. Circular presentation of the balanced Gray code (2.2).

Remark 8.2. The analysis of the case *abcba* (Section 8.1) and the symmetry of the *standard Gray code*, exhibited in Figure 14, have the following consequence. If w is a principal word of a balanced Gray code, isomorphic by permutations of letters to the standard one (2.2), and if Γ is a balanced Gray code which has w^{op} (the opposite of w) as a principal word, then Γ is also isomorphic to the standard code by permutation of letters. This allows us to test only the following words of length 5:

$$abcba \quad abaca \quad abcab \quad acbab \tag{8.2}$$

8.2. Principal word of the type ***abaca*****.** Let us continue by analysing the case when a principal word of the type *abaca*. Again by symmetry we can assume that $a = 1$, $b = 3$, $c = 2$ which means that the initial (known) part of Γ is shown in Figure 15.

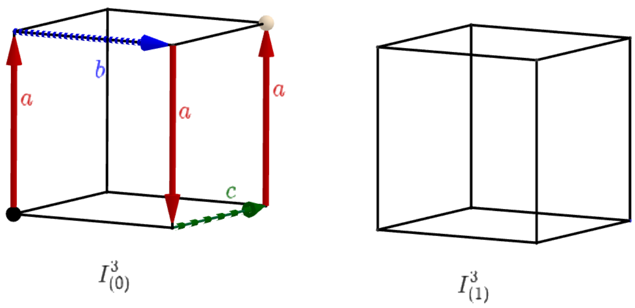

FIGURE 15. Principal word of the type *abaca*.

The question is how the word *abaca* can be continued.

We first observe that the remaining two vertices in the cube $I^3_{(0)}$ can be connected only by an edge of type $a = 1$. It immediately follows that in the cube $I_3^{(1)}$ we are allowed to use only steps $b = 3$ and $c = 2$. Considering that the sources (sinks) in $I_3^{(0)}$ and $I_3^{(1)}$ (the black and white vertices) should be matched, we observe that the only possible reconstruction of Γ is depicted in the Figure 16.

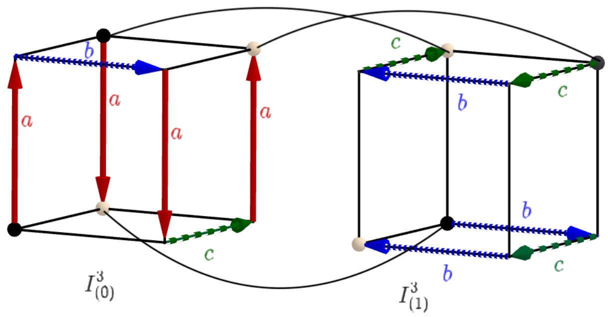

FIGURE 16. Unique reconstruction of the code in the case $w_1 = abaca$.

We obtain a code represented by the word

$$abaca(d)cbc(d)a(d)bcb(d)$$

which is isomorphic to the code (2.2). Indeed by interpreting letters a, b, c, d as $a = 4$, $b = 3$, $c = 2$ and $d = 1$ in Figure 16, we obtain the visual representation corresponding to code (2.2).

8.3. Principal words of the type $abcab$ and $acbab$. Let us first convince ourselves that $abcab$ can't be a principal word of any Gray code. Indeed, the corresponding path in the 3-cube $I^3_{(0)}$ disconnects the remaining two vertices, so they cannot be connected by w_3.

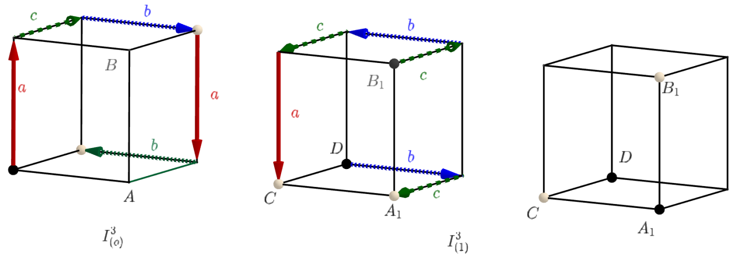

FIGURE 17. Principal word of the type $acbab$.

It remains to check the word $w_1 = acbab$. From the Figure 17 on the left, we observe that either w_3 begins at A and ends at B, or the other way around. We also observe that total letter count of w_1 and w_3 together is $LC(w_1, w_3) = (3a, 2b, c)$ (meaning that altogether there are 3 steps of type a, 2 steps of type b and one step of type c), which implies that the total letter count of w_2 and w_4 is $LC(w_2, w_4) = (a, 2b, 3c)$.

We conclude that there are two possibilities for the characteristic words w_2, w_3, w_4, depicted in Figure 17 on the right:

$$\text{(I)}\quad w_3 = \overrightarrow{AB} \quad w_2 = \overrightarrow{DA_1} \quad w_4 = \overrightarrow{B_1C};$$
$$\text{(II)}\quad w_3 = \overrightarrow{BA} \quad w_2 = \overrightarrow{DB_1} \quad w_4 = \overrightarrow{A_1C}.$$

The case (II) is not possible. Indeed, if $w_4 = \overrightarrow{A_1C}$ is of length 5, then it disconnects the vertices A_1 and D. If w_4 is of length 1 then w_2 is uniquely reconstructed, but its letter count is $(a, 3b, c) \neq (a, b, 3c)$.

In the case (I) the unique solution for the paths w_2 and w_4 is exhibited in the first cube in Figure 17 on the right. We obtain the code represented by the word

$$acbac(d)bc(d)a(d)cbca(d).$$

By permutation (bijection) $a \leftrightarrow b, c \leftrightarrow d$ we obtain a code with principal word $bdaba$, which is precisely the code shown in Figure 14.

8.4. Principal words of length four. For a principal word of length four, up to a permutation of letters and reversal of the order, there are two possibilities, $abca$ and $abac$. The word $abca$ is immediately ruled out since it disconnects the vertex-edge graph of the 3-cube.

If $w_1 = abac$, then either $w_3 = \overrightarrow{DC} = ab$ or $w_3 = \overrightarrow{CD} = ba$ (Figure 18). The letter count in both cases is $LC(w_1, w_3) = (3a, 2b, c)$. We observe that there are two possibilities:

(I) $w_2 = \overrightarrow{B_1D_1} = b$ and $w_4 = \overrightarrow{C_1A_1} = bcbab$;

(II) $w_2 = \overrightarrow{B_1C_1} = cac$ and $w_4 = \overrightarrow{D_1A_1} = aca$.

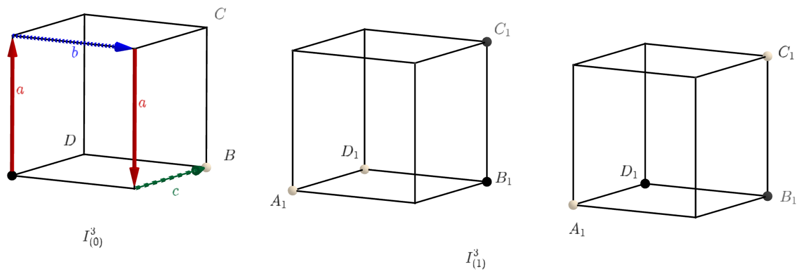

FIGURE 18. Principal word of the type *abac*.

The first case is not possible since w_4 is of length 5 (and $w_1 = abac$ is not principal. In the second case we have $LC(w_2 + w_4) = (3a, 0b, 3c)$ and the code is not balanced.

The final conclusion is that there are no balanced codes with a principal word of length four.

8.5. Characteristic word *abc* **is not possible.** In other words we claim that the word *dabcd* does not appear in a balanced 4-bit Gray code Γ. Suppose the opposite. We know that $\{a, b, c\} = \{1, 2, 3\}$, so for concreteness (symmetry) let $a = 1$, $b = 3$, $c = 2$ (Figure 19).

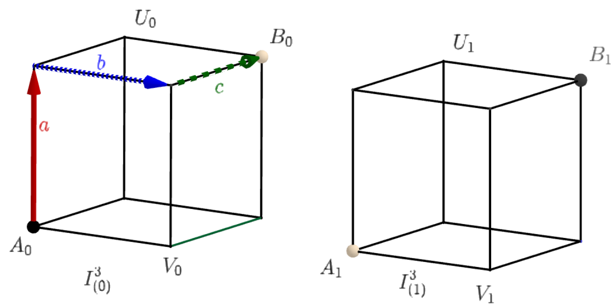

FIGURE 19. The case of the characteristic word *abc*.

Figure 19 records what we know so far. For example the sources/sinks (as indicated) are in the set $\{A_i, B_i, U_i, V_i\}_{i=0,1}$. Suppose that U_0 is the source and V_0 is the sink.

The only possible (two) ways to complete Figure 20 on the left to a Gray code is depicted on the right side of the figure.

We obtain two Gray codes but neither of them is balanced. The case when U^0 is the sink and V^0 is the source is similarly ruled out.

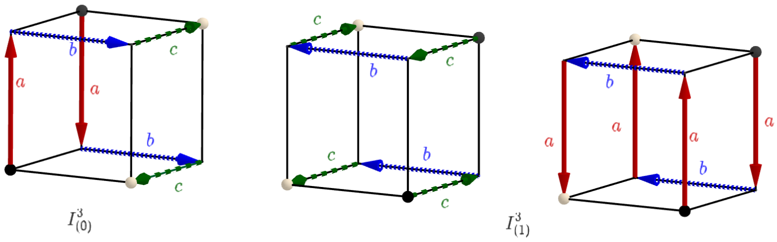

FIGURE 20. Two possible reconstruction of the code with the principal word abc.

8.6. Principal word aba is not possible. Since the principal word $w_1 = aba$ is of length three, all characteristic words are of length three. Observe that either $w_3 = aba$ or $w_3 = bab$.

If $w_3 = aba$ then the total letter count for w_1 and w_3 is $LC(w_1, w_3) = (4a, 2b, 0c)$ which implies that the total letter count for w_2 and w_4 is $LC(w_2, w_4) = (0a, 2b, 4c)$. It immediately follows that $\{w_2, w_4\} = \{cac, cbc\}$. The case $w_2 = cbc$ is not possible since $aba(d)cbc(d)$ is a cycle so we arrive at the word

$$aba(d)cac(d)aba(d)cbc(d)$$

which is not a Gray code.

If $w_3 = bab$ then the total letter count for w_1 and w_3 is $LC(w_1, w_3) = (3a, 3b, 0c)$ which implies that the total letter count for w_2 and w_4 is $LC(w_2, w_4) = (0a, 3b, 3c)$. It follows that $\{w_2, w_4\} = \{bab, cbc\}$. The case $w_2 = cbc$ is again not possible since $aba(d)cbc(d)$ is a cycle so we arrive at the word

$$aba(d)bab(d)bab(d)cbc(d)$$

which is again not a Gray code.

Acknowledgement. R. Živaljević was supported by the *Science Fund of the Republic of Serbia*, Grant No. 7744592, Integrability and Extremal Problems in Mechanics, Geometry and Combinatorics – MEGIC.

References

1. D. Avis, *Non-partitionable point sets*, Inform. Process. Lett. **19** (1984), 125–129.
2. S. Beckett, *Quad*, In: *Collected Shorter Plays*, Faber, London 1984.
3. K. B. Chilakammari, P. Hamburger R. E. Pippert. *Venn diagrams and planar graphs*, Geom. Dedicata **62** (1996), 73–91.
4. ______, *Hamilton cycles in planar graphs and venn diagrams*, J. Comb. Theory, Ser. B **67** (1996), 296–303.
5. F. Effenberger, W. Kühnel, *Hamiltonian, submanifolds of regular polytopes*, Discrete Comput. Geom. **43** (2010), 242–262.
6. E. N. Gilbert, *Gray codes and paths on the n-cube*, Bell. Syst. Tech. J. (1958), 815–826.
7. B. Grünbaum, *Partitions of mass–distributions and convex bodies by hyperplanes*, Pac. J. Math. **10** (1960), 1257–1261.
8. ______, *Venn diagrams and independent families of sets*, Math. Magazine **1**(1975), 12–23.
9. ______, *Venn diagrams I*, Geombinatorics **1**(1992), 5–12, 12–23.
10. H. Hadwiger, *Simultane Vierteilung zweier Körper*, Arch. Math. (Basel) **17** (1966), 274–278.

11. F. Harary, *Graph Theory*, CRC Press 2018, Westview Press 1969 (first edition).
12. P. Hamburger, R. E. Pippert *Simple, reducible Venn diagrams on five curves and Hamiltonian cycles*, Geom. Dedicata **68** (1997) 245–262.
13. ———, *Simple, reducible Venn diagrams on five curves and Hamiltonian cycles*, Math. Magazine **73** (2000), 105–110.
14. D. E. Knuth, *Combinatorial Algorithms, Part 1*, Upper Saddle River, New Jersey: Addison-Wesley, 2011, xvi+883pp.
15. W. Kühnel, C. Schulz, *Submanifolds of the cube*, In: P. Gritzmann, B. Sturmfels, B. (eds.) *Applied Geometry and Discrete Mathematics*, The Victor Klee Festschrift. DIMACS Series in Discrete Math. and Theor. Comp. Sci., vol. 4, pp. 423–432. Am. Math. Soc., Providence (1991).
16. G. Pruesse, F. Ruskey, *All Simple Venn Diagrams are Hamiltonian*, arXiv:1504.06651 [math.CO] (2015).
17. E. Ramos, *Equipartitions of mass distributions by hyperplanes*, Discrete Comput. Geom. **15** (1996), 147–167.
18. F. Ruskey, M. Weston, *A Survey of Venn diagrams*, Electron. J. Comb. https://www.combinatorics.org/files/Surveys/ds5/VennEJC.html.
19. G. C. Tootill., *Proc. IEE 103, Part B Supplement*, (1956), p. 435.
20. P. Winkler, *Venn diagrams: Some observations and an open problem*, Congr. Numerantium **45** (1984) 267–274.
21. F. Yao, D. Dobkin, H. Edelsbrunner, M. Paterson, *Partitioning space for range queries*, SIAM J. Comput. **18** (1989), 371–384.
22. G. M. Ziegler, *Shelling Polyhedral 3-balls and 4-polytopes*, Discrete Comput. Geom. **19** (1998), 159–174.
23. R. T. Živaljević, *Topological methods in discrete geometry*, Chapter 21 in: J. E. Goodman, J. O'Rourke, C.,D. Tóth (eds) *Handbook of Discrete and Computational Geometry*, third ed., CRC Press LLC, Boca Raton, FL, 2017.
24. ———, *Equipartitions of measures in* $\mathbb{R}^4$, Trans. Am. Math. Soc. **36**0 (2008), 153–169.

Faculty of Natural Sciences and Mathematics
University of Sarajevo
Sarajevo
Bosnia and Herzegovina
manuela@dizdarevic.org

(Received 01 12 2021)

Mathematical Institute SASA
Belgrade
Serbia
rade@mi.sanu.ac.rs